geologica acta

Citation: Sethy, P.C., Naik, A., Nayak, R., 2025. Geochemical characterization and tectonic significance of the granite gneiss in the Tikiba Granitic Complex, Northwest Odisha, India. Geologica Acta, 23.20, 1-pgs. DOI: 10.1344/GeologicaActa2025.23.20

Online ISSN: 1696-5728

Geochemical characterization and tectonic significance of the granite gneiss in the Tikiba Granitic Complex, Northwest Odisha, India

Pratap Chandra Sethy[1] Ashutosh Naik[2] Ranjit Nayak[3]

[1]**Wadia Institute of Himalayan Geology, Dehradun**
248001, Uttarakhand, India. E-mail: pratapwihg@gmail.com

[2]**Sambalpur University**
Burla, Sambalpur, Odisha, India

[3]**Faculty of Emerging Technologies, Sri Sri University, Cuttack**
754006, Odisha, India

ABSTRACT

The study explores the Precambrian tectonic evolution and the growth of continental crust in the southern region of the North Odisha Singhbhum Craton (NOSC), delving into the potential petrogenetic processes and source characteristics. The Tikiba Granitic Complex (TGC) is in the contact area of the Eastern Ghat Mobile Belt (EGMB) and the NOSC. The present study involves the geochemical characteristics of TGC granitoids and their geochemical variations. Petrographically, the TGC is comprised of alkali feldspar granite, monzogranite to granodiorite. The major element geochemistry reveals calc-alkalic, ferroan to magnesian affinities, and a metaluminous, peraluminous and peralkaline character. It is enriched in LILE and HFSE like Yb, Sm, Zr and Y. The $(La/Yb)_N$ values range from 4.0–26.1 and exhibit distinct negative Eu anomalies (Eu/Eu*) (0.4-0.6). This granitic complex shows high ∑REE contents of 176-860ppm with variable enrichment in LREE. Both REE and other incompatible element compositions define an A-type affinity. Based on geochemical data, we conclude that these granitoids have probably derived from a predominant crustal source with variable mantle characteristics in a post-orogenic setting.

KEYWORDS **Tikiba Granitic Complex. A-type granites. Post orogenic. Archean. Singhbhum Craton.**

INTRODUCTION

Craton-margin mobile belts exhibit play a crucial role in the evolution of continents through orogenesis, involving multiple phases of deformation and metamorphism (Ennih and Liégeois, 2008; St-Onge *et al*, 2009). These belts record the complex growth history of continents by documenting various tectonic processes such as metamorphism and structural reconfigurations. Craton-margin mobile belts exhibit a structurally complex assemblage of rocks with highly variable magmatic and metamorphic characteristics. Different regions of the continental crust have distinct lithological assemblages and geodynamic settings, but granitoids are most common rock types (Clarke, 1992; Pitcher, 1997; Tarney, 1984; Taylor and McLennan, 1981; Weaver and Windley, 1996; Winter, 2012). Diversity in occurrence and tectonic implications to different tectonic regimes makes the study of these granitoids a center of attention to the geoscience community (Moyen *et al.*, 2009).

The Singhbhum Province in northern Odisha, eastern India, features an Archaean cratonic core, which is tectonically enclosed by Mesoproterozoic metamorphic belts, specifically the Singhbhum Mobile Belt (SMB) (Sarkar *et al.*, 1962) and the Eastern Ghats Mobile Belt (EGMB) (Crowe *et al.*, 2003; Fig. 1). According to Saha (1994), six Precambrian crustal provinces are recognized in the Indian Shield. Among these, the North Odisha Singhbhum Craton (NOSC) and the Central Indian Craton (CIC) include the northwestern part of Odisha. The 200 km long Raigarh-Kamakhyanagar (R-K) lineament, extending from Raigarh (Chhattisgarh) in the west to Kamakhyanagar in the east, separates two distinct geological provinces. This lineament has been interpreted variously by different workers as the Sukinda Thrust (Rao, 1964), the North Odisha Boundary Fault (NOBF) (Mahalik, 1994, 1996), and the Kerjang Fault (Nash *et al.*, 1996). Detailed mapping of the R-K lineament points to this area is mainly composed of granitic rocks (Fig. 1) together with bands and lenses of low-grade supra-crustal rocks.

A review of the existing literature on the study area reveals that research on these granitoids has been relatively limited. The petrogenesis and tectonic significance of these granitoids is poorly understood. Investigating the geochemistry of these granites can help decipher their source characteristics, magma evolution, and geodynamic conditions. Thus, the field study, petrography, and geochemical data generated will be used to constrain the petrogenesis and understand the tectonic relevance concerning the crustal growth in the southern part of NOSC during the late Archean age. The data generated will be compared with other granitic bodies/complexes of NOSC, *i.e.* Bonai Granitic Complex (BGC), Kuchinda Granitic Complex (KGC), Jharsuguda Granite (JG), and Tamperkola Granite (TG) to understand the evolution of the TGC granitoids.

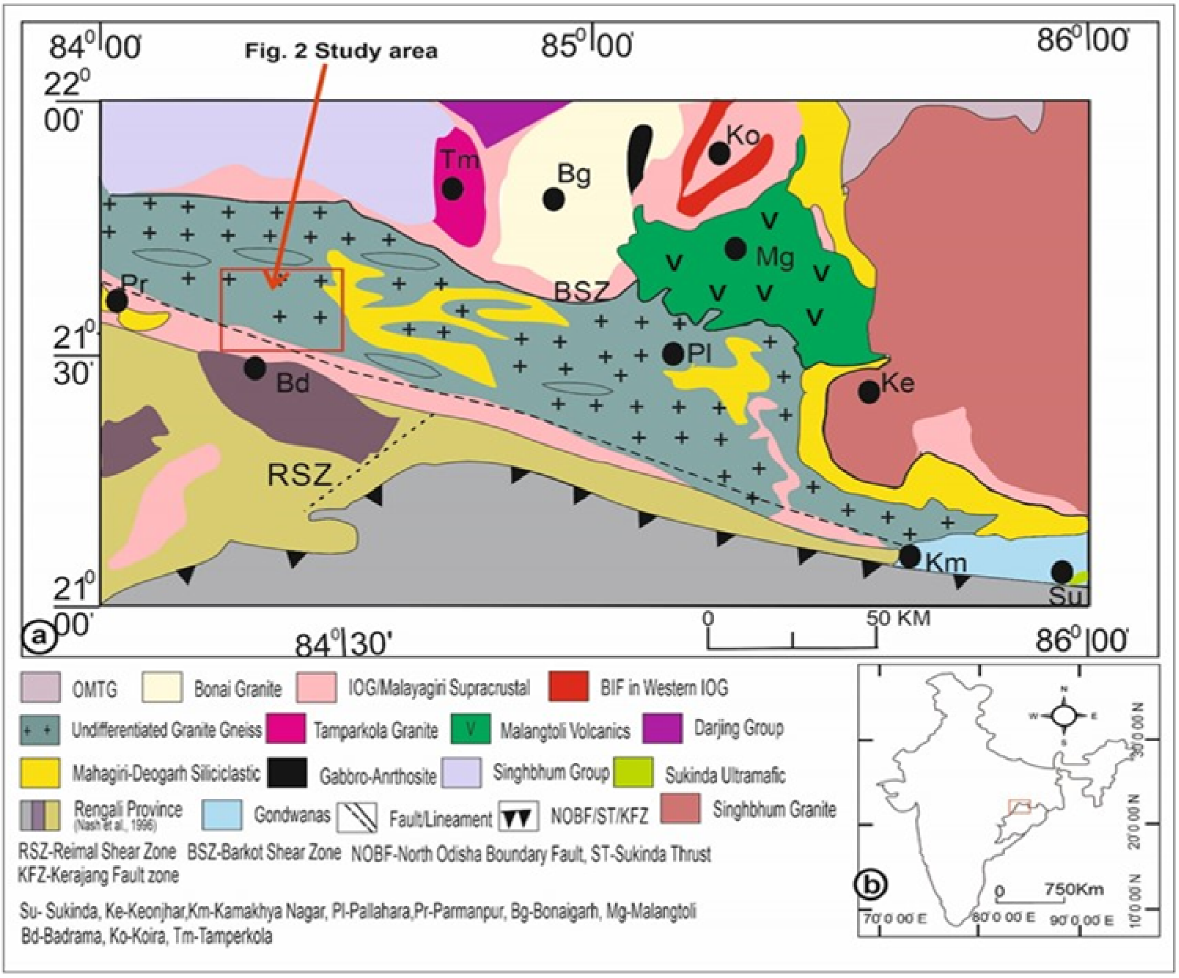

FIGURE 1. A) Geological map of Northern Odisha Singhbhum Craton (NOSC); B) Map of India showing the location of the study area.

DOI: 10.1344/GeologicaActa2025.23.20

GEOLOGICAL SETTING

The study area lies in the north-eastern part of Sambalpur district in Odisha (Fig. 2). An area bounded by N21°30' to N21°45' latitudes and E84°10' to E84°30' longitudes, covering ~869sq km, was mapped in detail on a 1:50,000 scale by Sethy (2014). The Singhbhum Craton is one such Precambrian terrain in eastern India that records sedimentation and volcanism in both convergent and divergent tectonic regimes spanning the Paleoarchean to Neoproterozoic (Eriksson *et al.*, 2006; Mukhopadhyay, 2001; Mukhopadhyay *et al.*, 2008; Mazumder, 2005; Mazumder *et al.*, 2000; Saha, 1994; Sarkar and Gupta, 2012). Nash et al. (1996) and Crowe et al. (2003) suggested that the Deogarh group is part of the Rengali Domain, with the northern part carved out of NOSC and the southern

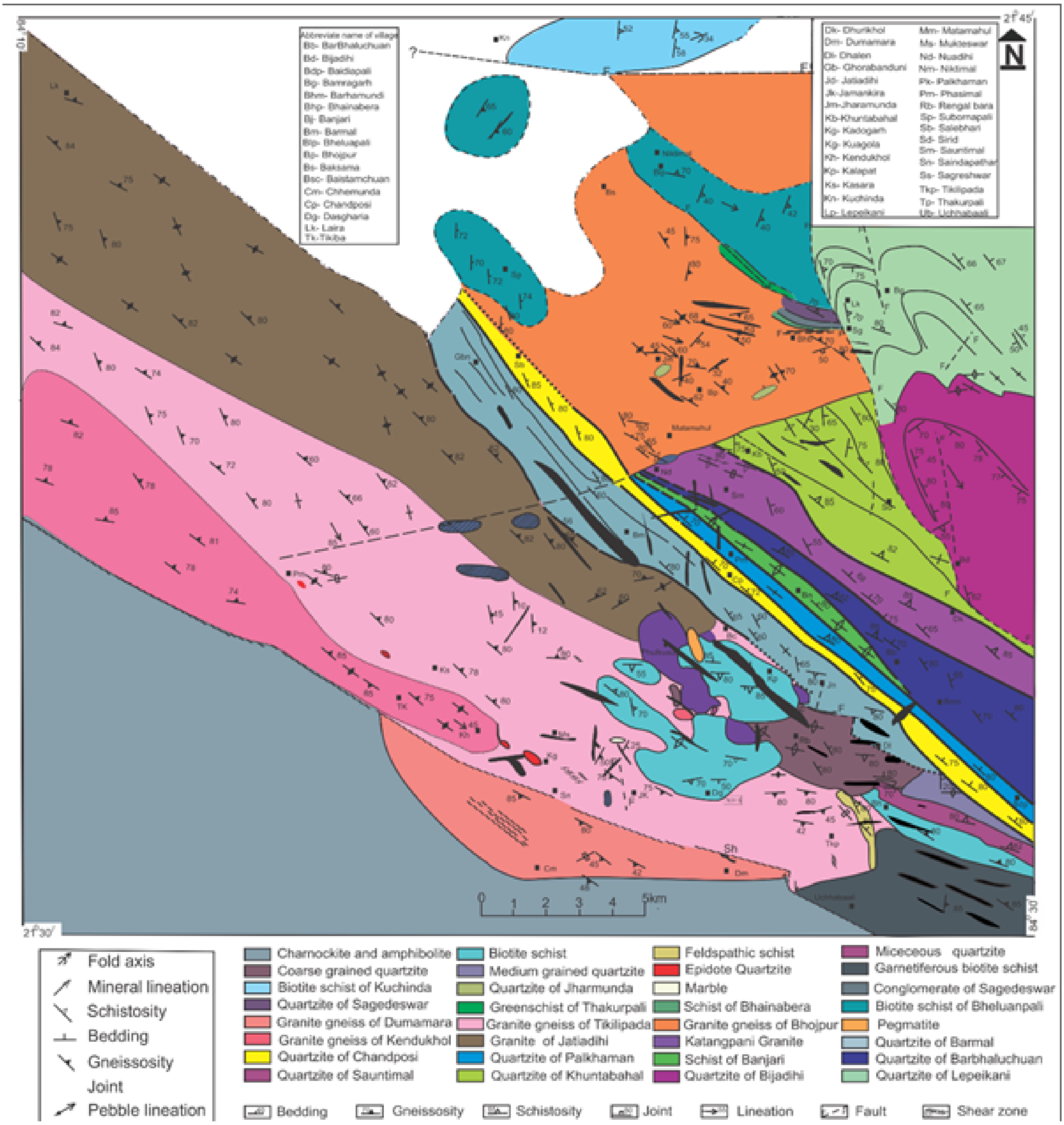

FIGURE 2. Geological map of the Tikiba Granitic complex, showing the major rock units (Sethy, 2014).

part from the EGMB. The EGMB is an orogenic belt characterized by high-grade granulite facies rocks. It is globally recognized as a polycyclic granulite terrain that has undergone intense multiphase deformation, making it one of the prominent high-grade metamorphic belts in the world.

The TGC is predominantly composed of Precambrian rocks, which include a diverse assemblage of low-grade metasedimentary and metavolcanic lithologies, along with intrusive granitic bodies (Rath *et al.*, 1993). The TGC was described earlier in geological literature as a part of unclassified granites (Mazumdar, 1978). The regional geological setting of TGC is such that it appears to form a southwestern continuation of Singhbhum granite (Mukhopadhyay *et al.*, 2020). The study area exposes mainly granite gneiss with metasedimentary units within this complex. This complex is mostly made of micaceous quartzite, medium-grained cross-bedded quartzite, coarse-grained quartzite, epidote-bearing quartzite, marble, garnet-bearing biotite schist, etc. In addition to the lithological diversity, the area is structurally complex, with numerous shear zones trending in both E-W and N-S directions. These shear zones transect and deform all the lithological units, indicating multiple episodes of tectonic activity that have significantly influenced the structural architecture of the TGC.

FIELD OBSERVATION AND PETROGRAPHY

The northern margin of the Singhbhum Craton, encompassing the Tikiba region of Southwest Odisha, that exposes a complex suite of Precambrian granitoid (Asokan et al., 2021; Saha, 1994 and references therein). The granitoids from the study area intrude into the older greenstone belts of the Precambrian. The TGC granite are mainly intruded into the supracrustal sequence of low to medium-grade metasedimentary rocks like quartzite, biotite schist, and phyllites. This granitic complex represents a composite intrusive body, consisting of multiple felsic to intermediate magmatic facies. These facies encompass porphyritic granites, gneissic components (migmatitic and augen gneisses), and dykes. These lithologies occur as distinct bodies as well as gradational assemblages. The granites are pink to grey in colour, medium to coarse-grained, and largely massive. Porphyritic texture with K-feldspar megacrysts is locally developed. Gneisses display prominent foliation and banding, with alternating quartz feldspathic and biotite-rich layers. The gneissic units show well-developed gneissosity and compositional layering, likely related to early deformation and often folded (Fig. 3A, C). In many outcrops of the Tikilipada Granite Gneiss (TGG), zebra banding is observed, which can be defined by the occurrence of inter-fingering pink and grey color bands which may vary in thickness up to 20mm. At some locations, this granitic body is observed to have a higher proportion of biotite (Fig. 3E). Moreover, the granite gneiss shows a dextral slip faulting (Fig. 3D). The style and geometry of the folds vary significantly across different exposures of Kendukhol Granitic Gneiss (KGG), ranging from gently plunging to vertical, and from open to isoclinal types (Fig. 3F). Several exposure of the KGG have, a prominent stretching of mineral lineation is developed on the foliation surface, typically parallel to the axes of certain fold axis. Weak foliation is observed in the Katangpani Granite (KG) indicating late-stage tectonic over-printing. Jointing is prevalent across all facies, and the general trend of these joints are NW-SE and NE-SW direction. The contacts between granite, and granite gneiss are varied, being both gradational and intrusive for instance sharp, chilled margins are occasionally noted where granite intrudes into gneisses, suggesting multiple intrusive phases. The rocks are often crosscut by pegmatite and aplite veins, which are common features in the complex (Pandey *et al.*, 2018).

Petrographic study of representative thin sections of TGC reveals that the rocks exhibit diverse mineral assemblages and textures that reflect their magmatic origin and varying degrees of deformation. The overall mineralogical composition of these granites gneiss is quartz (24-30%), K feldspar (microcline and orthoclase) (30-45%), plagioclase (25-35%), biotite (3-4%), muscovite (2-3%), hornblende (<2%) with accessory minerals such as titanite, acmite, epidote, monazite, zircon, and opaque minerals. Quartz mainly occurs as aggregates of smaller grains within alkali feldspar phenocrysts which are anhedral to subhedral (Fig. 4A-C, E). The plagioclase grains exhibit very faint lamellar twinning, and their composition varies from albite to oligoclase. Some of the plagioclase grains are completely sericitized (Fig. 4A, B). Due to deformation, some of the large grains of plagioclase have recrystallized into aggregates of tiny grains with sutured contacts. The microcline grains (0.1 to 1.5mm) are subhedral and crosshatched twins (Fig. 4E). Hornblende shows a typical bright green color in plane -polarized light position which is typically found in Tikilipada and Bhojpur granite gneisses (Fig. 4D). Tiny flakes of biotite are scattered throughout the rock, generally occurring in the intergranular spaces and sometimes enclosed within the microcline. Slender muscovite flakes occur in between larger quartz and feldspar grains. Some biotite flakes are altered to chlorite along the cleavage planes and margins (Fig. 4B. F).

METHODOLOGY

The TGC samples were collected from the western parts of Odisha covering NOSC. For the whole-rock major

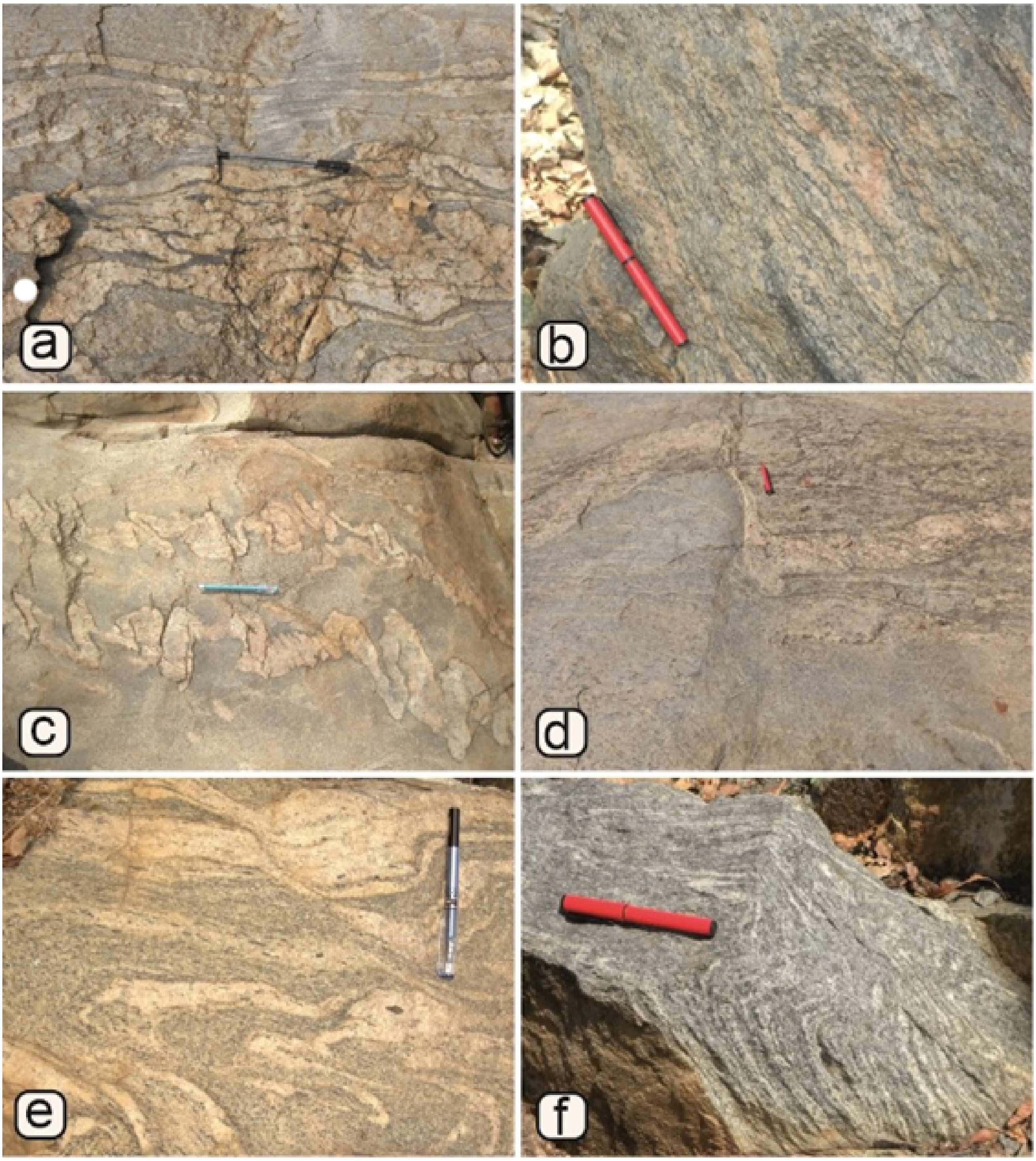

FIGURE 3. Photograph showing A) The pegmatitic veins intruded into the TGG along the gneissosity plane and both gneissosity and pegmatite veins have folded each other. B) Medium to coarse-grained TGG are well gneisses; C) Pegmatitic veins, injected into gnessisity plane, deformed in ptigmatic folds observed in TGG granite; D) Dextral shearing with a faulting plane in a granite gneiss; E) Planner view of compositional layering of TGG; and f) tight to isoclinal plunging fold in the KGG.

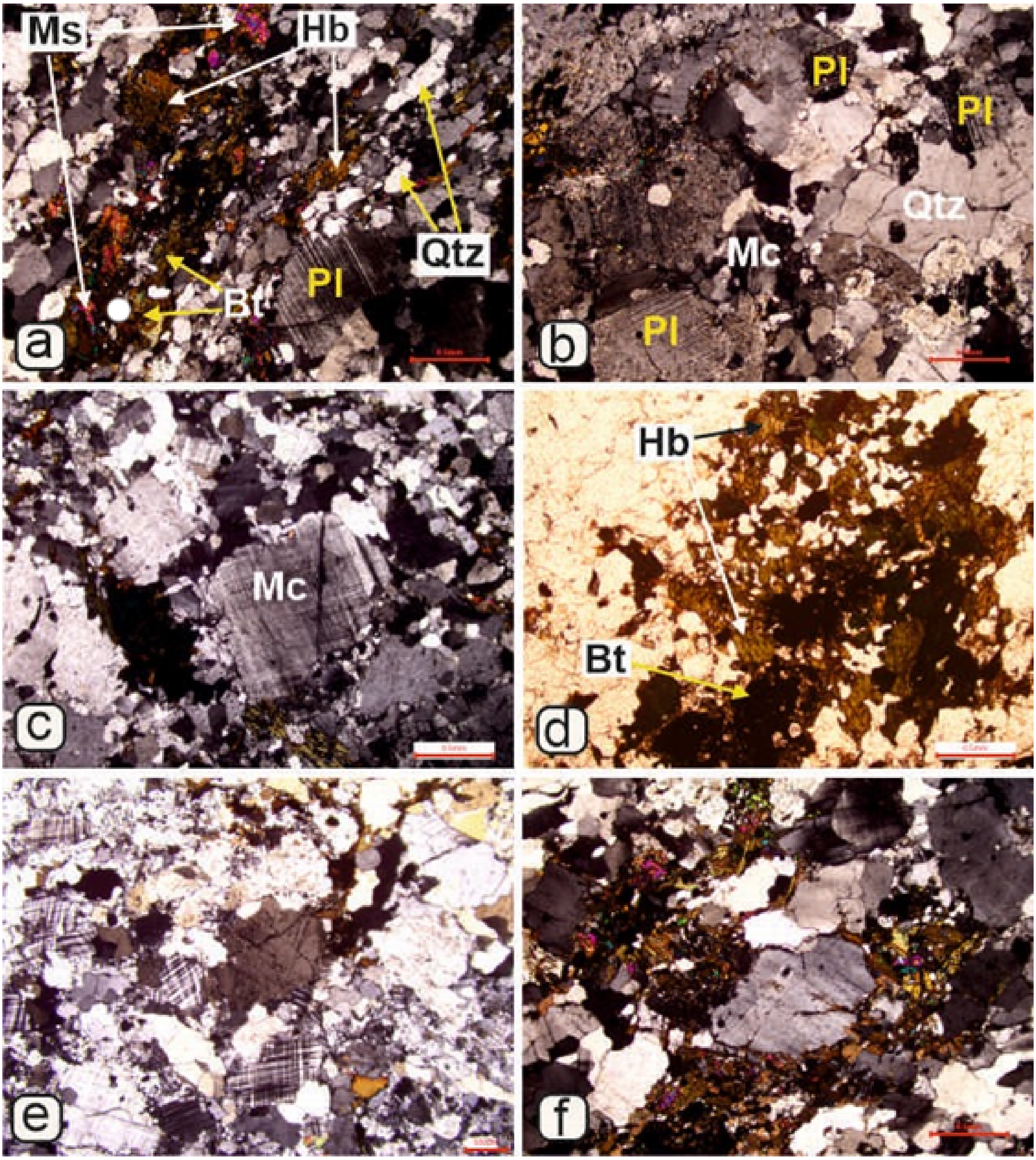

FIGURE 4. Photomicrographs of TGC in XPL A) TGG sample displaying porphyritic texture with plagioclase exhibiting lamellar twinning and elongated quartz grains at the gneissosity plane; B) Some of the plagioclase grains are completely sericitized and chess-board twinning of Microcline (Mc); C) Phenocrysts of alkali feldspar and two types of quartz grains exhibiting anhedral to subhedral texture; D) A typical bright green hornblende is a common feature in both the TGG. The provided photomicrograph is representative of the TGG rock; E) Microcline grain showing crosshatch twinning; F) Biotite grains are alter into chlorite. The undeformed feldspar and quartz grains shows the inequigranular texture, indicate a magmatic origin with limited post-crystallization deformation. Qtz: Quartz; Pl: Plagioclase; Mc: Microcline; Ms: Muscovite; Bt: Biotite; Hb: Hornblende.

oxides and trace elements data, the rock samples were powdered using an agate disc-incorporated laboratory disc mill, which was then converted into pellets. The major oxides (SiO_2, Al_2O_3, MgO, Na_2O, K_2O, CaO, TiO_2, P_2O_5, MnO and Fe_2O_3) along with some trace elements (Zn, Ga, Sr, Pb, Sc, Co, Ni, Ba, Cr, V, Cu, Zr, Rb, Y and Nb) were analyzed at Wadia Institute of Himalayan Geology (WIHG), Dehradun, India, using X-ray fluorescence (XRF) spectroscopy (Bruker S8 TIGER). The error percentage for analysing the trace elements is between ±2 and ±3% and for the major oxides between ±5 and ±6%. Calibration coefficients for the analyses were derived using a model given by Lucas-Tooth et al. (1964). The Loss On Ignition (LOI) was estimated by heating 5g of the powdered rock sample to 150°C to remove the adsorbed water present in the rock samples, and followed by heating the samples at 850°C. The analytical precision and accuracy of the sample preparation and instrumental performance were calculated using international reference materials such as JSP-1 (USGS)-granite, MB-H and JG-2 (GS Japan)-granite.

The Rare Earth Elements (REEs), and a few trace elements like Th and U, were analysed using the Inductively Coupled Plasma-Mass Spectrometer (ICP-MS) PerkinElmer SCIEX ELAN RDC-e in the same institute (Wadia Institute of Himalayan Geology (WIHG), Dehradun, India. Approximately 0.1g of powdered sample (<200mesh) was mixed with 20mL of HF and HNO_3 (2:1 ratio) and 2mL of $HClO_4$ in Teflon crucibles. The Teflon crucibles were heated by using a hot plate and the rock samples were fully digested to get a dry paste of the sample. This was followed by the addition of 20mL of 10% HNO_3 to the sample and then left on a hot plate for 10-15minutes until a clear solution was obtained. The clear solution was made up to 100ml final volume with milli-Q water and analysed by ICP-MS. The accuracy range for REE analysis is 2-12% with precision varying from 1-8% as discussed by (Saini *et al.*, 2007, 2014) and Khanna (2009).

RESULTS

Geochemistry

The Tikiba granitic complex comprises five main magmatic facies or variants that are distinguishable based on their field relation, texture, and composition, as well as both mineralogical and chemical characteristics. These include 1. Tikilipada Granite Gneiss (TGG), 2. Kendukhol Granite Gneiss (KGG), 3. Bhojpur Granite Gneiss (BGG), 4. Jatiadihi porphyritic Granite Gneiss (JGG) and 5. Katangpani syno Granite (KG). The whole rock geochemistry data is given as supplementary files S1 and S2.

Tikilipada Granite Gneiss (TGG)

The major element chemistry of the TGG aligns with monzogranite displaying high SiO_2 content which ranges varies from 74.2-77.0wt% (avg. 75.7wt%) and Al_2O_3 varies from 10.6-11.8wt% (avg. 11.2wt%) (Table 1). The TAS diagram shows the granitic nature of the studied samples (Fig. 5). The Modified Alkali-Lime Index (MALI) diagram displays the alkali-rich and evolved nature of the TGG (Fig. 6). In general, they show metaluminous to mildly peraluminous character with molecular A/CNK [Al_2O_3/($CaO+Na_2O+K_2O$)] values of 0.94-1.02 (Fig. 7). The normative composition of the granite is predominantly quartz and orthoclase (Table 2). These rocks are primarily sodic in composition and albitic, except KG (K_2O/Na_2O< 8.0) and Na_2O+K_2O is avg. 6.28. The studied granite exhibits Ga/Al and Fe/Mg ratios of 1.03 and 1.97 (avg. values), respectively. On a chondrite normalized REE diagram (Fig. 8), TGG exhibits moderately fractionated REE patterns (avg. La/Yb= 10.67) and negative Eu anomaly (Eu/Eu*= 0.49) and Sr/Y values (avg. 1.26). In the primitive mantle normalized diagram (Fig. 9), the studied rocks exhibit weak negative anomalies like Ba, Sr and Nb, along with inconstant enrichment of Large Ion Lithophile

TABLE 1. Representative major oxides data of TGC

	TGG				KGG				BGG				JGG				KG			
Sample	79TKP	134MT	53BF	Avg. n=8	KH136	Tkp-23	TKP-25	Avg. n=12	BP-9	BP-10	BP-18	Avg. n=10	JGG/1	103JT	272JT	(Avg. n=6)	500 BP	KP/2	KP3/A	Avg. n=6
SiO_2	77	76,5	75,6	75,7	75,4	73,1	72,5	73,5	75,7	75,1	72,7	73,3	73,3	73,1	71,5	73,3	73,2	73,2	74,1	73,9
TiO_2	0,2	0,3	0,2	0,6	0. 35	0,4	0,5	0,5	0,3	0,3	0,6	0,4	0,3	0,2	0,2	0,2	0,2	0,6	0,2	0,3
Al_2O_3	11,4	11,4	11,5	11,2	10,9	11,2	11,9	11,4	10,4	11	9,8	10,8	14,3	14,3	15,6	14,5	14,7	14	14,2	14,1
Fe_2O_3	2,4	2,4	3,3	2,5	3,7	4,5	4,7	4,4	3	2,9	4,3	3,9	1,9	2	2,1	1,9	1,6	1,4	1,6	1,7
MgO	0,2	0,2	0,2	0,5	0,3	0,5	0,6	0,4	0,3	0,2	0,5	0,3	0,9	0,4	0,4	0,5	0,5	0,8	0,4	0,5
CaO	2,6	2,6	2,5	2,5	1,3	2,5	2,1	1,8	1	0,9	2	1,4	0,5	0,6	0,6	0,6	0,9	0,9	0,9	0,8
Na_2O	0,9	0,9	0,8	0,8	2,7	2,2	2,1	2,5	3,3	3,3	2,2	3	3,7	3,4	2,9	3,2	3	3,8	3	3,2
K2O	5,2	5,3	5,5	5,4	4,8	4,4	4,3	4,7	5,6	5,6	7	6,3	4,9	5,9	6,1	5,2	5,6	4,8	5,4	5,2
P_2O_5	0	0	0	0,1	0,1	0,2	0,2	0,1	0,1	0,1	0,1	0,1	0	0,1	0,1	0,1	0,1	0,2	0,1	0,1
MnO	0,03	0,03	0,03	0,1	0,1	0,1	0,2	0,1	0,05	0,05	0,1	0,1	0,08	0,01	0,01	0	0,02	0,06	0,02	0
Total	99,9	99,43	99,51	99,5	99,09	99,09	98,97	99,21	99,57	99,49	99,36	99,4	99,74	99,85	99,51	99,5	99,74	99,63	99,88	99,7
feoT	2,15	2,15	2,96	2,3	3,32	4,04	4,22	3,95	2,69	2,6	3,86	3,5	1,7	1,79	1,88	1,7	1,43	1,25	1,49	1,5
Mg#	14,16	14,16	10,71	24,2	13,83	18,04	20,18	14,49	16,53	12,02	18,72	11,6	48,41	28,37	27,39	31,2	38,23	53,09	33,12	35,9
A/Nk	1,6	1,57	1,58	1,5	1,13	1,33	1,46	1,15	0,9	0,95	0,87	0,9	1,25	1,19	1,37	1,3	1,33	1,22	1,31	1,3
A/CNK	0,96	0,95	0,97	0,9	0,9	0,86	0,99	0,91	0,78	0,83	0,66	0,8	1,16	1,09	1,25	1,2	1,16	1,07	1,14	1,1
K_2O/Na_2O	5,77	5,88	6,87	6,5	1,77	2	2,04	1,85	1,69	1,69	3,18	2,2	1,32	1,73	2,1	1,6	1,86	1,26	1,8	1,7

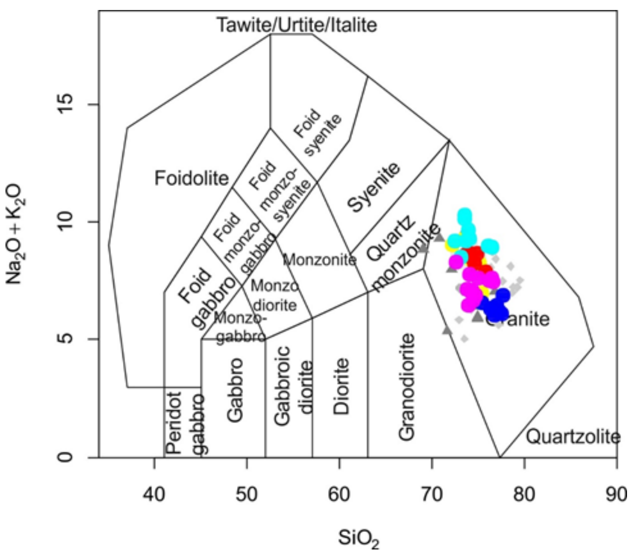

FIGURE 5. SiO_2 versus K_2O+Na_2O diagram for the TGC (after Le Bas *et al.*, 1986). The grey symbols indeed represent comparative geochemical data for various granites from the Singhbhum Craton, which are presented to provide a regional context for our studied samples. These include: Bamara granite: (Chaki *et al.*, 2005); Jharsuguda granite: (Pandey *et al.*, 2018); Pallahara granite: (Topon *et al.*, 2018) and Bonai granite: (Asokan *et al.*, 2023).

Elements (LILE) and depletion of High Field Strength Elements (HFSE) (Table 3).

Kendukhol Granite Gneiss (KGG)

The KGG represents a silica-rich suit of granodiorite rocks with SiO_2 ranging from 72.5-76.0wt%, and Al_2O_3 contents between 10.1 and11.9wt% (Table 1). In the TAS diagram, the studied samples fall in the field of granite (Fig. 5). On the Alumina Saturation Index (ASI) diagram (Fig. 7), the granite samples plot within the metaluminous field. The rocks are characterized by high total alkali contents (Na_2O+K_2O= 6.0-10.2wt%) and notably low concentrations of CaO (0.4-2.9wt%) and MgO (0.1-1.0wt%). The normative mineralogical composition of the rock is predominantly quartz and feldspar (Table 2). The KGG is sodic in composition, with K_2O/Na_2O ratios <2.01 and an average total alkali content (Na_2O+K_2O) of 7.21wt%. In contrast, the TGG exhibits higher K_2O/Na_2O ratios (<8.0) and a lower average total alkali content of 6.28wt%. Moreover, KGG samples display lower concentrations of incompatible trace elements such as Rb (144-171.8ppm) and Y (28.0-54.0ppm) compared to the TGG and other granitic units in the study area. The studied granite exhibits Ga/Al and Fe/Mg ratios of 1.44 and 3.48 (avg.), which are higher than the TGG. The Sr/Y concentration of this granite (avg. 1.47) is higher than the TGG (avg. 1.26) and lower than KG (avg. 2.29). On a chondrite normalized REE diagram (Fig. 8), the KGG is comparatively poorer in REE (avg. ΣREE= 561ppm) as compared to the TGG (650ppm). These granites are less fractionated than TGG with an average $(La/Yb)_N$= 7.8 and exhibit negative europium anomaly (Avg. Eu/Eu*= 0.6). In the primitive mantle normalized diagram (Fig. 9), the KGG is enriched in LILE and depleted in HFSE. These rocks have pronounced negative Ba, Sr and Nb anomalies.

Bhojpur Granite Gneiss (BGG)

The alkali feldspar BGG is a silica-rich granitoid with a restricted range (SiO_2: 71.4-75.7wt%) (Table 1). Characteristically, these rocks have a high content of total alkalis (avg. 9.22wt%) and K_2O content (5.5-7.0wt%) is higher than Na_2O (2.2-3.4wt%). This rock samples are essentially peralkaline in composition with A/NK and A/CNK ratios in the range of 0.9-1.0 and 0.7-0.8 respectively. A positive association between A/NK and A/CNK suggests fractionation of plagioclase (Fig. 7; Maniar and Piccoli, 1989). The rock has normative aegirine mineral (Morimoto *et al.*, 1988) which is not found in other varieties of TGC granites (Table 2). They have low Mg# (5.1 to 18.7) when compared to the KGG (7.6 to 20.9) and TGG, and are high in incompatible elements such as Rb (153-222ppm), Y (32-121ppm) etc. The average Ga/Al (1.72) and Fe/Mg (4.03) ratios of the studied granite are higher than those observed in the TGG and KGG. These rocks are enriched in the LREEs [$(La/Sm)_N$= 3.7-5.7] and depleted in the HREEs $(Eu/Yb)_N$= 0.5-0.7) resulting in fractionated REE patterns with high $(La/Yb)_N$= 5.5-6.9 ratio (Table 3). Europium anomaly is subtle to moderate (Eu/Eu*= 0.4-0.5) and the $(Ce/Sm)_N$ ratios are low (2.6-3.3). The Nb (42-80.0ppm),

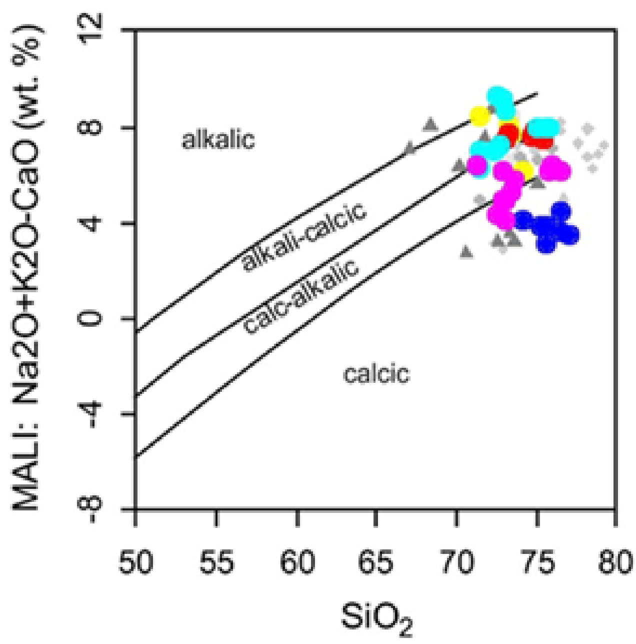

FIGURE 6. Na_2O+K_2O-CaO vs. SiO_2 (%) plot (Frost *et al.*, 2008).

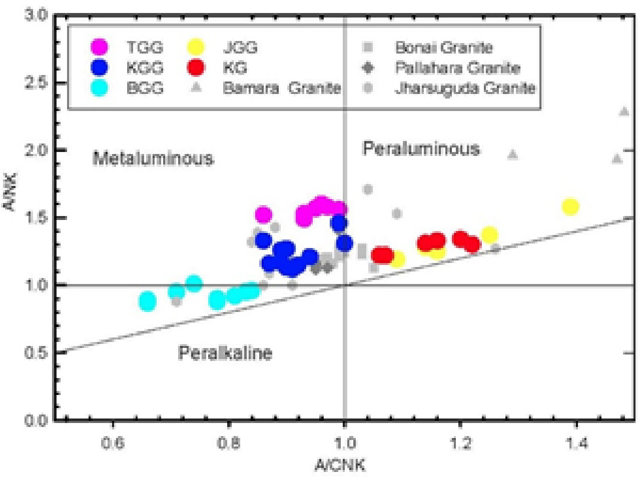

FIGURE 7. A/NK vs. A/CNK plot (Maniar and Piccoli, 1989).

Rb (153-222ppm) and Y (32.5-121.0ppm) content are moderately high while the Sr/Y ratios (avg. 1.09) are lower than the studied granitic rocks. All the BGG samples are characterized by negative Nb, Sr and Y anomalies in multielement diagram (Fig. 9).

Jatiadihi porphyritic Granite Gneiss (JGG)

The major oxide data, with CIPW norms (Table 1) reveals that the Jatiadihi samples are porphyritic granite gneiss. This granite exhibits variable composition with moderate to high silica (SiO_2 ranging from (71.5-74.2wt%) and Al_2O_3 (13.9 -15.6wt%) and low concentration of CaO (0.5 to 1.12wt%), MgO (0.35 to 0.60wt%), TiO_2 (0.16 to 0.24wt%), MnO (0.01 to 0.09wt%) and P_2O_5 (0.01 to 0.13wt%). The concentration of Fe_2O_3 (1.8-2.1wt.%) and MgO (0.3-0.9wt.%) are low along with TiO_2, MnO and P_2O_5. These gneisses have a peraluminous composition according to the alumina saturation index A/CNK, which ranges from 1.1 to 1.4 (Fig. 7). The JGG is potassic, with K_2O values as high as 6.1wt% and K_2O/Na_2O is (avg. 2.01) and a high Mg# (22.1-48.4) in comparison to the BGG (5.1 to 18.7). The average Ga/Al (1.08) and Fe/Mg (2.22) ratios of the studied granite are higher than the TGG and lower to BGG and KGG. The chondrite normalized REE diagram (Fig. 8) shows that the JGG has an average ΣREE content of 189ppm. This granite is less fractionated than BGG (605ppm) and TGG (649.84ppm) and exhibit negative europium anomalies (avg. Eu/Eu*= 0.4). The primitive mantle normalized diagram shows a relative Rb, Th, U and Pb enrichment, and Ba, Nb, Sr and Zr depletion (Fig. 9). The Zr (139-270ppm), Rb (33-342ppm), and Y (26-91ppm) content in these rocks is moderately high, while exhibiting the Sr/Y ratios (0.55-2.96) are low (Table 3). Interestingly, the gneiss exhibits high concentrations of Pb (54ppm) and Th (342ppm).

Katangpani syno Granite (KG)

The major element contents of KG (Table 1) reflect their homogeneous composition. They contain high silica (73.2-75.1wt%), 4.6-5.7wt% K_2O, 3.0-3.8wt% Na_2O and 7.0-8.7wt% total alkali (K_2O+Na_2O). Figure 5 shows the total alkali-silica (TAS) diagram of studied samples classified as granite (Le Bas et al., 1986). The samples of KG are high in Al_2O_3 (13.6-14.7wt%), and shows peraluminous signatures (A/CNK= 1.06-1.22; Fig. 7). The KG has low MgO (0.4-0.8wt%), with Mg# varying in between 28.37-53.09 (avg. 31.2) and JGG (avg. 35.9). The normative composition of the granite is peraluminous in nature and dominant quartz, feldspar, and corundum as accessory mineral (Table 2). These rocks display high concentration of Cr (<41.0ppm) and Ni (12.0-26.0ppm) and show negative Eu anomaly (Eu/Eu*= 0.40-0.51) with high ΣREE values ranging from 545 to 565ppm. However,

TABLE 2. Normative mineralogical composition of TGC

	TGG				KGG				BGG				JGG				KG			
Samples	79TKP	134MT	53BF	Avg. n=8	KH136	Tkp-23	TKP-25	Avg. n=12	BP-9	BP-10	BP-18	Avg. n=10	JGG/1	103JT	272JT	Avg. n=6)	500 BP	KP/2	KP3/A	Avg. n=6
Q	46.26	45.44	44.44	44.39	39.89	38.67	39.01	37.31	34.99	33.94	32.02	31.29	30.62	29.15	29.69	33.00	31.93	30.18	32.75	33.41
C	0.00	0.00	0.00	0.05	0.00	0.00	0.45	0.06	0.00	0.00	0.00	0.00	2	1.46	3.37	2.60	2.31	1.40	2.02	2.00
Or	30.73	31.32	32.50	32.36	28.37	26.00	25.41	27.68	33.09	33.09	41.37	36.99	28.95	34.86	36.04	30.73	33.09	28.37	31.91	30.93
Ab	7.62	7.62	6.77	7.19	22.85	18.62	17.77	21.65	22.32	25.40	11.43	20.73	31.30	28.77	24.53	27.22	25.39	32.16	25.39	26.94
An	11.71	11.41	11.54	10.38	3.45	7.69	9.11	5.79	0.00	0.00	0.00	0.04	2.48	2.32	2.32	2.71	3.81	3.16	3.81	3.23
Ac		0		0	0			0	4.94	2.22	6.33	3.95	0	0	0	0	0	0		0
Di	0.93	1.08	0.67	1.00	1.61	2.65	0.00	1.48	1.61	1.08	2.69	1.40	0	0	0	0	0	0		0
Wo		0.04	0.00	0.10	0.12	0.00	0.00	0.13	0.93	1.02	2.43	1.81	0	0	0	0	0	0		0
Hy	0.07	0.00	0.19	0.66	0.00	0.02	1.50	0.27	0.00	0.00	0.00	0.00	2.24	0.99	0.99	1.16	1.25	1.99	1.00	1.20
Mt	0.10	0.10	0.10	0.30	0.33	0.33	0.65	0.35	0.16	0.16	0.33	0.24	0.32	0	0	0.05	0.00	0.33	0.00	0.11
Hm	2.33	2.33	3.23	2.34	3.48	4.28	4.25	4.16	1.18	2.02	1.89	2.40	1.67	2	2.1	1.91	1.60	1.18	1.60	1.61
Ap	0.00	0.00	0.00	0.27	0.24	0.47	0.47	0.28	0.24	0.24	0.24	0.26	0	0.23	0.23	0.16	0.24	0.47	0.24	0.24
Sum	99.74	99.34	99.44	99.03	100.32	98.72	98.62	99.16	99.47	99.17	98.72	99.12	99.61	99.81	99.31	99.55	99.61	99.22	98.71	99.66

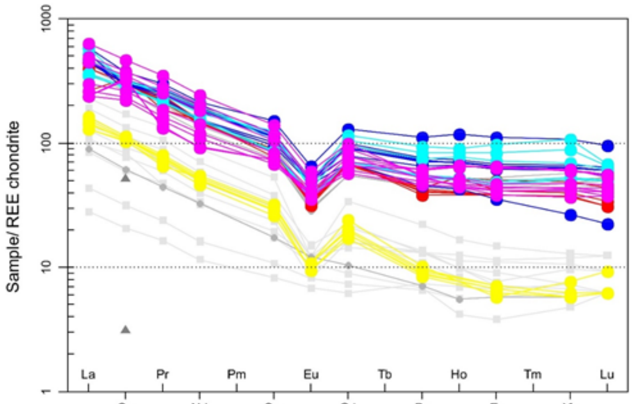

FIGURE 8. Chondrite-normalized Rare Earth Element (REE) patterns for A type TGC (Normalization values are from Sun and McDonough (1989)).

there are the variable concentration of the trace elements in these granites such as Sc (3-14ppm), Rb (1-84ppm), V (8-28ppm), Zn (18-40), Ga(14-21ppm) and moderate amounts of Y (17-61ppm), Nb (24-51ppm), and Th (28-195ppm). Ba (477-995ppm), Zr (124-201ppm), Cr (28-41ppm) and Sr (38-99ppm) shows relatively moderate values. For the studied granite, average Ga/Al and Fe/Mg ratios are 0.97 and 0.99, respectively, which are lower than those of TGG, KGG, BGG and JGG. The chondrite-normalized REE patterns enrichment (Fig. 8) and show high fractionation of $(La/Yb)_N$= 5.41-12.26, and $(Ce/Yb)_N$= 6.83-8.15 ratios. The Primitive mantle normalized plots show distinct positive anomalies of Th and U and negative anomalies of Ba, Nb and Sr (Fig. 9).

DISCUSSION

Classification

Based on the source rock type and the pressure-temperature conditions during melting, granitoids are often classified into four types: S, I, A and M (Chappell and White, 1974). According to Loiselle and Wones (1979), Whalen et al. (1987) and Eby (1990), there have been multiple efforts to differentiate A-type granites from other types. Additionally, various geochemical discrimination diagrams have been developed for this purpose, such as those proposed by Pearce et al. (1984) and Whalen et al. (1987). The geochemical attributes of the current study granitoids align precisely with those of typical A-type granites (Figs. 10; 11; 12A, B). The studied rock of TGG and BGG are ferroan but JGG and KG are magnesium-rich and KG samples exhibit low concentrations in Mg and Fe (Fig. 10). The KGG is calcic, while the Bhojpur, Jatiadihi, Katangpani and Tikilipada granite gneiss exhibits a calc-alkalic composition (Fig. 6).

Diverse discrimination diagrams are employed to delineate the genetic context of granites and effectively distinguish the types of granites. In the (Y+Nb)-Rb and Y-Nb plots proposed by Pearce et al., (1984), the TGC samples plot in the Within-Plate Granite (WPG) field (Fig. 11). The attributes of high Na_2O+K_2O (avg. 7.94), molar Ga/Al (avg. 1.27) and Fe/Mg (avg. 2.74) ratios, low CaO content, enrichment in HFSEs, and depletion in Eu and Sr are considered to play a significant role in discriminating A-type granites (Bonin, 2007; Collins *et al.*, 1982; King *et al.*, 1997; Loiselle and Wones, 1979; Whalen *et al.*, 1987). Therefore, it can be concluded that the studied samples showing the high concentrations of HFSEs and elevated 10,000×Ga/Al ratios (>2.6) further support their classification as A-type granites. This is also evident in the Zr vs. 10,000×Ga/Al diagram (Fig. 12A) and the Nb vs. 10,000×Ga/Al plot, (Whalen *et al.*, 1987; Fig. 12B) Further it can be stated that the studied samples consistently fall within the A-type granite field in multiple geochemical discriminant plots (Fig. 13A, B), reinforcing their A-type affinity. These granites are notably alkali-enriched, as indicated by high total alkali contents (K_2O+Na_2O)(avg. 7.94), elevated $(Na_2O+K_2O)/CaO$ ratios (avg. 7.12) and dominant K_2O over Na_2O. They also exhibit high REE (except Eu) and HFSE elements such as Y, Th, Zr and Ga accompanied by noticeable depletion of Sr, Nb, Ba, P and Eu (Fig. 9). Additional evidence is observed in the Y/Nb vs. Ce/Nb plots (Fig. 13A), where the TGC granites predominantly align with the average continental crust.

Petrogenesis

After Loiselle and Wones (1979) coined the term A-type for granite, several magmatic processes have been proposed to explain the formation of A-type granites. These include partial melting of the crust (Huang *et al.*, 2008; Jung *et al.*, 1998, 2000), magma mixing between basaltic

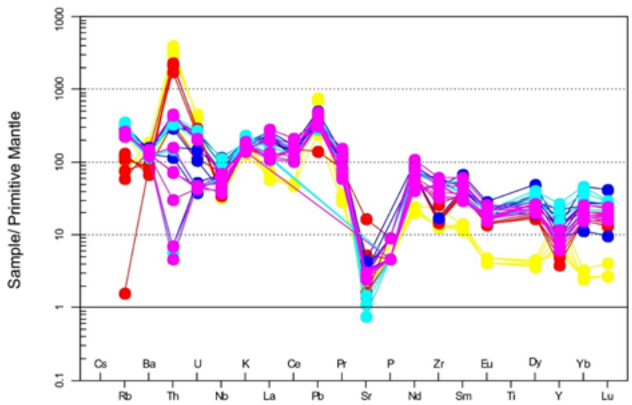

FIGURE 9. Primitive-mantle normalized trace element spider diagrams for the A type TGC granites. The normalization values are from Sun and McDonough (1989).

DOI: 10.1344/GeologicaActa2025.23.20

TABLE 3. Trace element composition of TGC

	TGG				KGG				BGG				JGG				KG			
Sample	79TKP	134MT	53BF	Avg. n=8	KH136	Tkp-23	TKP-25	Avg. n=12	BP-9	BP-10	BP-18	Avg. n=10	JGG/1	103 JT	272 JT	Avg. n=6	500 BP	KP/2	KP3/A	Avg. n=6
Ba	1136	1086	1022	970.6	1059	855	881.5	939.3	878	803	850	842.9	592	621	551	748.6	661.4	570	603.5	641.2
Cr	33	33	24	35.3	20	42.5	40.5	31.1	48	34.6	37	39.8	12	40	35	33.8	34.9	28	38.8	35
V	11	20	26	19.7	14	20	16	16.1	10	7.1	15	13	10	12	14	10.5	15	28	12.5	14.4
Sc	4	6	5	4.6	4	1.3	1.6	3.1	4	2.9	4.7	4.3	6	4	4	4.2	6.5	14	4	6
Co	2.6	6.7	<1.0	3.8	4.4	0.4	2	3.7	<1.0	<1.0	4.3	4.5	138	2.7	3.2	25.4	3.8	4.5	3.5	3.7
Ni	17	21	22	13.1	13	2.6	3.5	6.2	16	20	8.2	12.8	11	15	14	13.9	20.3	12	23	21
Cu	17	21	54	25.6	10	25	14	12.4	14	18	17	17.4	4	13	16	12.7	17.5	1	23	18.5
Zn	48	86	149	104.1	80	122	94	78.5	96	90	91	92.6	73	38	42	45.4	34.1	18	39.5	35
Ga	18	18	21	15.8	18	6	4.5	11.9	21	30	8	16.3	19	21	23	21.4	18.5	14	20	18.7
Pb	21	36	35	26.4	31	25.5	23.9	27.1	31	35	20.5	26.2	17	54	49	45.9	24.3	10	29	25
Th	25	34	34	18	38	0.6	0.4	16.1	28	36	0.6	17.5	33	237	342	243.8	150.3	28	191	156.7
Rb	146	186	209	175.1	144	170	167	161.3	222	208	156	180.4	159	69	70	79.4	48.1	1	69.3	52.9
U	2.2	4.3	5.3	2.9	4.3	0.9	1	2.1	4.4	5.8	0.9	2.7	2.4	9.5	8.4	7.9	5.1	2.4	6	5.2
Sr	66	93	65	68.7	61	60	56.5	59.1	16	31.5	60	45.3	50	42	46	44.9	113.3	357	32	99.5
Y	41	59	102	59.3	53	28	31.5	41.8	69	121	34	60.9	91	26	33	48.7	38.3	61	27.8	35.7
Zr	194	525	696	564.1	546	681	588.5	513.1	590	502	582	567.4	276	139	149	165.7	291.9	653	171.5	272.4
Nb	29	53	82	54.2	50	49.1	36.8	39.3	48	80	42.1	51.6	51	23	24	28.1	31.9	51	24.5	30.9
La	161.4	182.9	148.4	151	74.9	197.7	153	107	143.7	184	109.4	133.6	40	50.4	40.6	44.9	124.7	81.9	139	127
Ce	241	300.4	216.3	247.8	268.4	379.2	307.8	260.6	264.7	250	227.1	240.8	84.4	91	83.4	86.9	249.2	269.3	242.6	248.3
Pr	28.8	36.9	27.2	31.2	16.2	42.6	34.7	24.4	29.8	33.4	26.1	28.5	7.9	9.9	8.4	9	26.7	22.9	28	26.8
Nd	91.2	128.9	92.9	111.2	56.3	145.6	123	85.4	103.3	125.9	91.1	102	31.8	33.1	27.6	30.8	88.6	90.4	88	88.3
Sm	18.5	29.6	19.8	22.4	14.3	27.1	22.9	17.5	24.4	20.5	16.7	19.3	6	6.3	5.1	5.8	16.4	16.3	16.5	16.5
Eu	3.4	4.8	3.5	3.7	2.6	4.4	3.8	3.2	3.1	3.6	2.7	3	0.8	0.8	0.7	0.8	2.5	2.9	2.4	2.5
Gd	17.9	33.4	20.6	24.3	16.9	25.8	23.2	19.2	24.8	30.1	18.3	22.3	6.2	5.3	4.4	5.1	17.9	18.4	17.8	17.9
Tb	2.7	6	3.5	3.9	3.1	3.5	3.4	3	4.2	5.5	2.9	3.7	1.2	BDL	BDL	1.2	2.9	2.9	BDL	2.9
Dy	14.6	36	20.9	23.6	20	17.5	18.1	17.7	24.1	30.2	17.3	21.6	3.3	3.1	2.7	3	14.2	17.6	13	14
Ho	3.1	8.5	4.8	5.2	4.8	3.2	3.6	3.8	5.6	6.5	3.7	4.7	2.1			2.1	3.8	3.8		3.8
Er	7.5	23.2	13	14.1	13.3	8	9.3	10.4	15.1	20.3	9.9	13.3	1.2	1.5	1.3	1.4	8.7	10.4	8.1	8.6
Tm	1	3.7	2.1	2.2	2.1	1.2	1.5	1.7	2.4	3.3	1.7	2.2	1	BDL	BDL	1	1.6	1.6	BDL	1.6
Yb	5.6	22.5	12.6	13.4	12.8	7.7	9	10.1	14.5	22.6	10.7	14.1	2.1	1.3	1.2	1.4	8.3	10.2	7.7	8.2
Lu	0.72	3.09	1.78	1.93	1.7	1.2	1.4	1.5	2	2.2	1.6	1.8	0.8	0.2	0.2	0.3	1.1	1.4	1	1.1
Eu/Eu*	0.57	0.47	0.53	0.49	0.51	0.51	0.5	0.54	0.39	0.44	0.47	0.44	0.4	0.42	0.45	0.4	0.45	0.51	0.43	0.4
LaN/YbN	19.43	5.48	7.94	8.63	3.95	17.31	11.46	7.75	6.68	5.49	6.89	6.53	16.85	26.14	22.81	23.6	10.13	5.41	12.17	10.7
LaN/SmN	5.49	3.89	4.71	4.295	3.29	4.59	4.2	3.73	3.7	5.65	4.12	4.35	4.19	5.03	5.01	4.9	4.78	3.16	5.3	4.8
CeN/YbN	11.13	3.45	4.44	5.34	5.42	12.74	8.85	6.95	4.72	2.86	5.49	4.71	13.64	18.11	17.98	17.5	7.77	6.83	8.15	7.9
CeN/SmN	3.14	2.45	2.64	2.69	4.53	3.38	3.24	3.65	2.62	2.94	3.28	3.05	3.39	3.49	3.95	3.6	3.67	3.99	3.55	3.6
EuN/YbN	1.73	0.61	0.79	0.871	0.58	1.62	1.2	0.95	0.61	0.45	0.72	0.63	1.42	1.75	1.66	1.7	0.86	0.81	0.89	0.9
Sum_REE	593.72	810.19	581.78	649.84	502.2	860	709.8	560.88	655.1	729.3	534.6	605.05	183.5	202.9	175.6	189.1	562.1	545.5	564.1	560.4

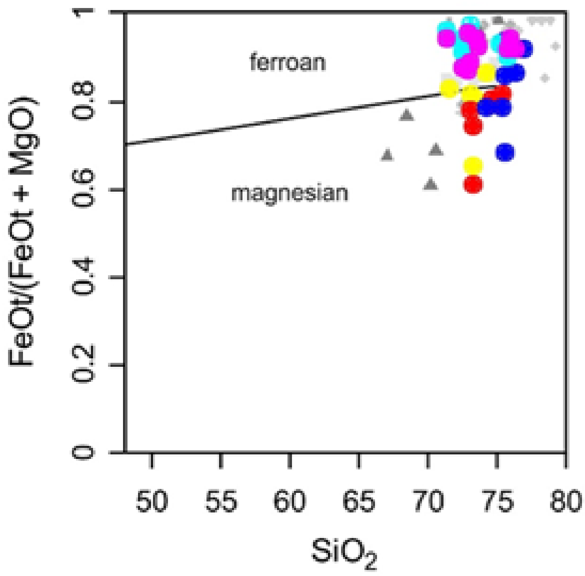

FIGURE 10. $FeO_t/(MgO+FeO_t)$ (%) vs. SiO_2 (%) plot Frost *et al.* (2001).

and crustal melts (Dall'Agnol and de Oliveira., 2007; Heilimo *et al.*, 2014; Yang *et al.*, 2006; Zhu *et al.*, 2010) and extensive fractional crystallization of a mantle-derived mafic magma with or without crustal contamination (Anderson *et al.*, 2003; Eby, 1990; Han *et al.*, 1997; Zhang and Zou, 2013; Zhong *et al.*, 2007). However, using discrimination diagrams of Eby (1992) based on trace element concentrations and their ratios (Ce/Nb vs. Y/Nb, Rb/Nb vs. Y/Nb). A-type granites were classified into A1 and A2 type. The differentiation of melts with compositions comparable to Oceanic Island Basalts (OIB) in the intraplate environment and continental rift setting is thought to be the source of the A1 type. It is noted that the A2 type (Eby, 1992) represents melts from a variety of sources, such as island arc basalts and continental crust. The Y/Nb ratio is one of this division's primary criteria. However, the Tikiba granitic complex is classified as A2 type due to its high Y/Nb ratios (>0.7) (Fig. 13B).

The formation of A-type granitoid has been attributed to three primary petrogenetic pathways: i) partial melting of crust, which includes amphibolites, charnockites, felsic granulites, and tonalites-granodiorites (Du *et al.*, 2016; Gorring *et al.*, 2004; King *et al.*, 2001), ii) differentiation of tholeiitic, transitional, or alkaline basalt (McCurry *et al.*, 2008; Namur *et al.*, 2011) and iii) crustal assimilation and fractional crystallization of basalt (Frost *et al.*, 1999; Mingram *et al.*, 2000). The lack of associated mafic to intermediate members and restricted chemical composition of the TGC preclude fractional crystallization of basalt as a main mechanism for their formation. According to this scheme, the TGC is classified as a metaluminous-peraluminous-peralkaline to calc-alkalic variation, resulting from the partial melting of the crust (Fig. 7). The major and trace elements composition displayed typical characteristics of A-type granite and showed strong enrichment of Rb, K, La, Ce, Zr, Nd and e.g. depletion of Sr, and P (Collins *et al.*, 1982; Whalen *et al.*, 1987). The enrichment of HFSE like Zr, Nb and REE elements that are commonly elevated in A-type granites. The TGC samples exhibit enrichment of REE, Rb, K, La, Ce, Zr and Nd elements (Fig. 8; 9) which is a typic character of A-type granites. Interestingly, the JGG

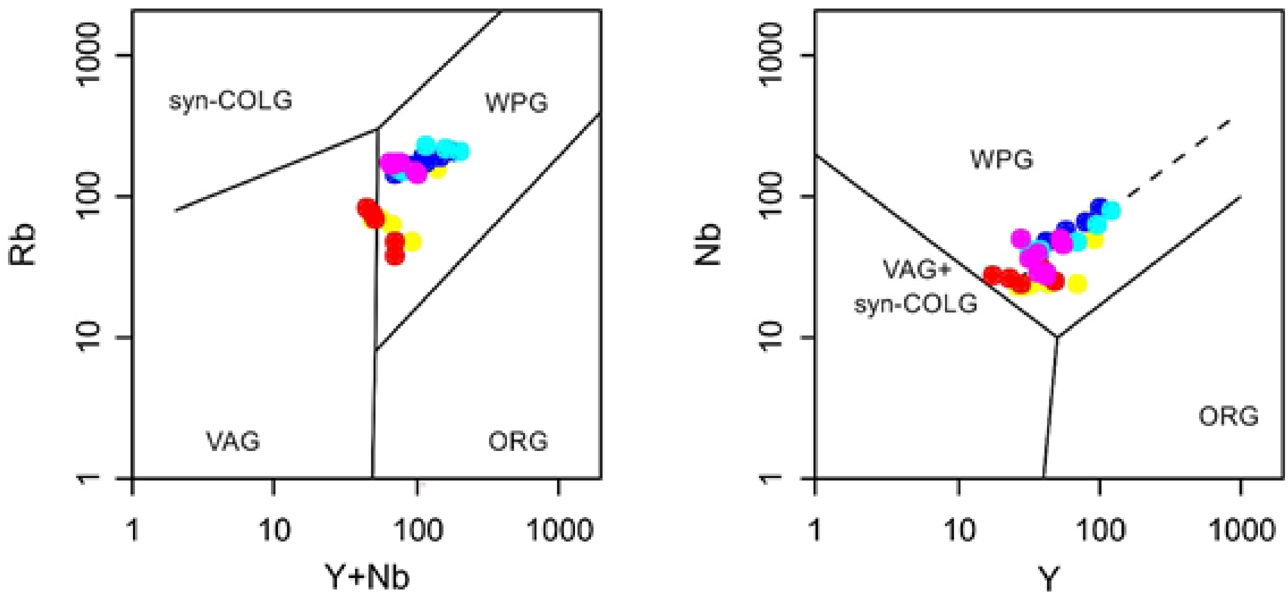

FIGURE 11. Tectonic setting discrimination diagram Rb versus Y+Nb and Y versus Nb (after Pearce *et al.*,1984). VAG= Volcanic Arc Granite; WPG= Within-Plate Granite; syn-COLG= syn-Collision Granite; ORG= Ocean Ridge Granites.

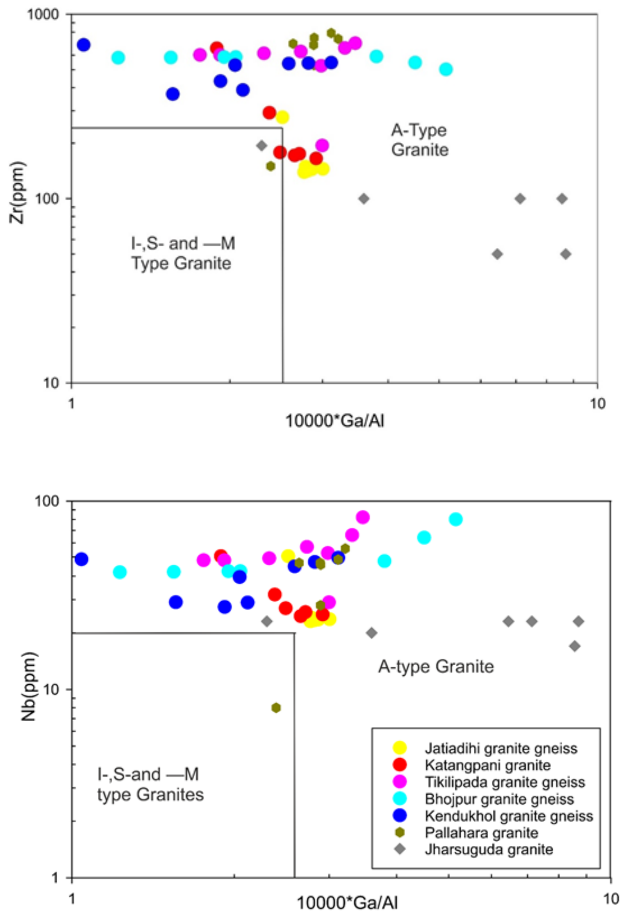

FIGURE 12. A) Zr or B) Nb, vs. 10,000×Ga/Al for A type TGC (after Whalen *et al.*, 1987).

has K_2O/Na_2O ratios quite high (1.3 to 2.1), suggesting to be a peraluminous A-type granite.

The Katangpani granite is geochemically distinct from the JGG and, based on field relationships, is observed to intrude the older JGG, signifying a younger magmatic pulse, likely associated with post-collisional or A-type granite settings. The inter-fingering pink and grey bands represent zones of differential crystallization of TGG and suggests the rock has a polyphase deformational history, likely linked to regional ductile shearing and metamorphism (Fig. 3E). The major element chemistry of the samples, when plotted in an $Al_2O_3/(FeO+MgO)^{-3}$×CaO^{-5}×(K_2O/Na_2O) ternary diagram after Laurent et al. (2014), suggests that metasedimentary rocks a possible source (Fig. 14). Additionally, the studied samples are high in Pb (54ppm) and Th (342ppm) content which implies mantle and crustal source mixing during the emplacement of these granitoids. However, the ternary diagram shown by Laurent et al. (2014) was unable to quantify the contributions of crustal and mantle sources to the genesis of granites. Consequently, to distinguish the proportional contributions of mantle and crustal sources in the TGC, several trace element ratios that are responsive to crust-mantle differentiation are formulated and analyzed in relation to the studied samples. Eby (1990) speculates that the A1 group is distinguished by trace-element ratios akin to those seen in OIB. The A2-type granite is distinguished by the variation of trace-element concentrations between the continental crust and island-arc basalts. These A2 granites represent magmas derived from the continental crust underplated during continent-continent collision. The incompatible element, Rb predominantly exists in crustal material, in contrast to mantle rock, which is often enriched in Heavy Rare Earth Elements (HREEs). The Y/Nb and Rb/Nb ratios of the analyzed samples fall within the A2 type granite domain, indicating that the TGC was formed during a continent-continent collision (Fig. 13B). However, the studied samples exhibit an average Rb/Sr value of 2.90, which is significantly higher than the typical values for mantle rocks (0.01 to 0.1; Taylor and McLennan., 1995). This stark contrast suggests that the genesis of the TGC involved a substantial contribution from lower crustal rocks rather than a mantle-derived source. Furthermore, the Sr/Y ratios of the studied rocks ranges from 0.55 to 2.96 (Table 3), that supports the interpretation of a shallow

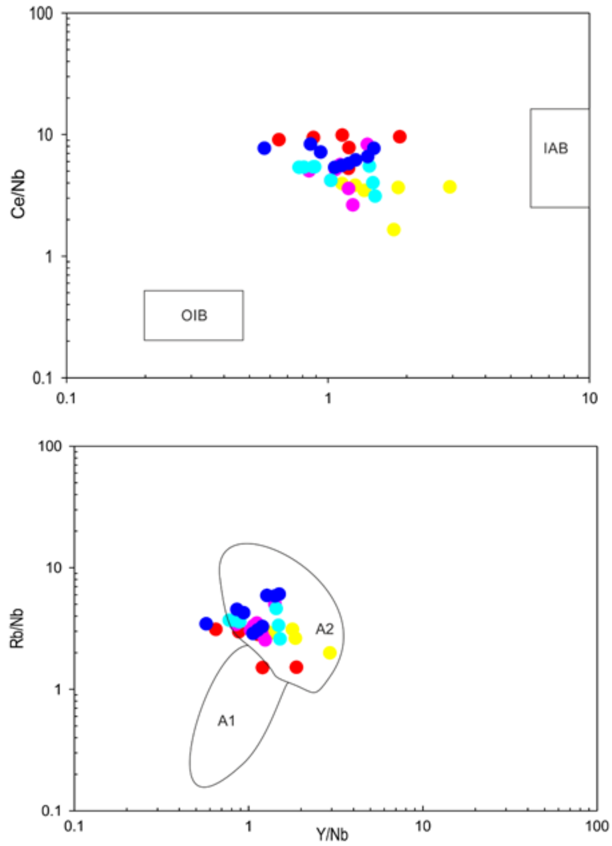

FIGURE 13. A) Tectonic discrimination diagrams (after Eby, 1992), TGC are closer to the field of island arc basalt than that of ocean island basalt field. B) Y/Nb vs. Rb/Nb diagram The TGC plots in the A2-type field.

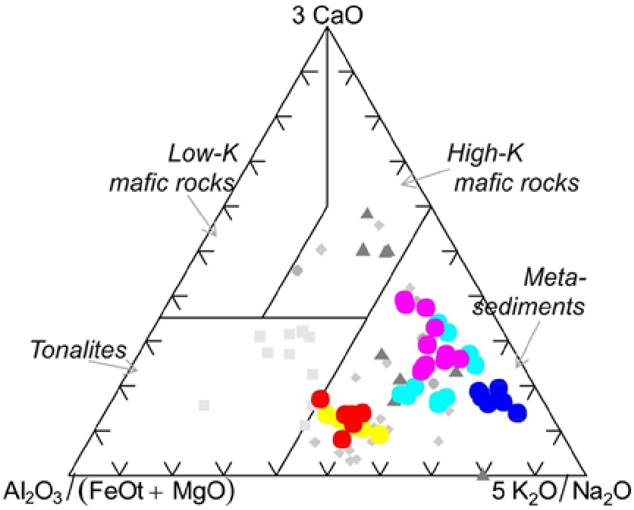

FIGURE 14. Ternary diagram (after Laurent *et al.* (2014) shows the sedimentary source of TGC.

crustal and garnet-free source (García-Arias *et al.*, 2024). This is consistent with partial melting under low-pressure conditions and aligns with an anorogenic tectonic setting.

Tectonic implications

A-type granites are well recognized as genetically associated with extensional or non-compressional regimes, forming in both post-orogenic and/or anorogenic settings (Barbarin, 1999; Collins *et al.*, 1982; Eby, 1992; Whalen *et al.*, 1987, 1996). A-type granites are typically categorized either to within-plate settings (A1) or to post-collisional settings (A2). Certain studies indicate that A-type geochemical characteristics can also occur in granites formed in confined extensional environments (Ashwal *et al.*, 2002; Eby, 1992; Pandit *et al.*, 2021; Wang *et al.*, 2018, 2020b; Whalen *et al.*, 1987). Geochemically and tectonically analogous extensional granites have been reported by numerous researchers from the Pallahara (Topon *et al.*, 2018), Bamara (Chaki *et al.*, 2005), and Jharsuguda (Pandey *et al.*, 2018) granitoids within the Singhbhum Craton. Based on the synchronous extensional A-type granite activity found in various parts of NOSC witnessed a juvenile crust and showed the Neoarchean A-type granite. Moreover, juvenile arc-related materials might have been involved in the genesis of the A-type granites which are genetically related to pot-orogenic settings (*e.g.* Goodge and Vervoort, 2006). Nonetheless, the high zirconium content (~180ppm), elevated Nb/Y ratios (1.75ppm), and enriched HFSEs, contradicts the involvement of juvenile mantle-derived material, as elevated zirconium abundances are typically associated with felsic, evolved and reworked crustal sources rather than juvenile magma (*e.g.* Bea, 1996; Kemp *et al.*, 2007; Miller *et al.*, 2003; Kemp *et al.*, 2007). The affinity of the studied A-type granites to A2- type in various discrimination diagram like Rb/Nb versus Y/Nb (Eby, 1992); (Fig. 13A, B) provides a first-order constraint that these granitoids might have formed in a post-collisional extensional setting. A comparative study of the REE and multi-element spider diagrams (Figs. 8; 9) of both the granites i.e. (Pallahara, Bonai, Jharsuguda, Tamperkola) and the A-type granite of this study indicate similar geochemical characteristics.

CONCLUSION

The southern margin of the Singhbhum Craton is the TGC, a magmatic entity embedded in the Archean crust. Based on the field studies, petrography, and whole-rock geochemical data the following conclusions can be drawn for the TGC- i) The petrographic and field characteristics of silica, and potassium-rich granitoids contain a diverse mineralogy, including hornblende, acmite, and corundum, and exhibit resorbed feldspar megacrysts. ii) These granitoids compositionally vary from alkali feldspar granite to granodiorite. The geochemical composition of these granitoids is peraluminous to peralkaline and ferroan to magnesian in character, displaying high contents of REEs and LILEs, suggesting their A-type (A2-subtype) affinity. iii) The geochemical evidence suggests the involvement of juvenile arc-related components in these granitoids. Furthermore, the high zirconium concentration (~180ppm) points to a substantial contribution from evolved, reworked crustal sources rather than exclusively mantle-derived juvenile inputs. iv) Overall, the geochemical characteristics of these rock types indicate their post-orogenic setting, with signatures of a 'Within-Plate' type tectonic environment.

ACKNOWLEDGMENTS

Dr. Pratap Chanadra Sethy is grateful to the UGC, New Delhi for providing financial assistance through the Rajiv Gandhi National fellowship (F14-2(Sc)/2007(SA-III). This paper also forms a part of the Ph.D. research work of PCS. The authors are also grateful to the Director of Wadia Institute of Himalayan Geology (WIHG), Dehradun for encouragement and for providing the necessary facilities to carry out this research work. PCS is also thankful to P. P. Khana, WIHG, Dehradun for the geochemical analysis.

CONFLICT OF INTEREST

The authors declare that they do not have any conflict of interest.

REFERENCES

Anderson, I.C., Frost, C.D., Frost, B.R., 2003. Petrogenesis of the Red Mountain pluton, Laramie anorthosite complex, Wyoming: Implications for the origin of A-type granite. Precambrian Res, 124, 243-267.

Ashwal, L.D., Demaiffe, D., Torsvik, T., 2002. Petrogenesis of Neoproterozoic granitoids and related rocks from the Seychelles: The case for an Andean-type arc origin. J Petrol, 43, 45-83.

Asokan, A.D., Mohan, M.R., Mahapatro, S.N., Shankar, R., Rasheed, K., 2023. Petrogenesis of metavolcanics and detrital zircon geochronology of the Mesoarchean western Iron Ore Group supracrustals, Singhbhum Craton (India): Evidence for an intracontinental extension setting. Precambrian Research, 396, 107157.

Barbarin, B., 1999. A review of the relationships between granitoid types, their origins, and their geodynamic environments. Lithos, 46(3), 605-626.

Bea, F., 1996. Residence of REE, Y, Th and U in granites and crustal protoliths; implications for the chemistry of crustal melts. Journal of petrology, 37(3), 521-552.

Bonin, B., 2007. A-type granites and related rocks: Evolution of a concept, problems and prospects. Lithos, 97(1-2), 1-29.

Chaki, A., Bhattacharya, D., Rao, J.S., Chaturvedi, A.K., Bagchi, A.K., 2005. Geochronology of the granitoids of the Kunjar Area, Sundergarh District, Orissa: Implications to the regional stratigraphy. Geological Society of India, 65(4), 428-440.

Chappell, B.W., White, A.J.R., 1974. Two contrasting granite types. Pacific Geology, 8, 173-174.

Collins, W.J., Beams, S.D., White, A.J.R., Chappell, B.W., 1982. Nature and origin of A-type granites with particular reference to southeastern Australia. Contrib Miner Petrol, 80, 189-200.

Crowe, W.A., Nash, C.R., Harris, L.B., Leeming, P.M., Rankin, L.R., 2003. The geology of the Rengali Province: Implications for the tectonic development of northern Orissa, India. Journal of Asian Earth Sciences, 21(7), 697-710.

Dall'Agnol, R., de Oliveira, D.C., 2007. Oxidized, magnetite-series, rapakivi-type granites of Carajás, Brazil: Implications for classification and petrogenesis of A-type granites. Lithos, 93(3-4), 215-233.

Du, L., Yang, C., Wyman, D.A., Nutman, A.P., Lu, Z., Song, H., Ren, L., 2016. 2090-2070 Ma A-type granitoids in Zanhuang Complex: Further evidence on a Paleoproterozoic rift-related tectonic regime in the Trans-North China Orogen. Lithos, 254, 18-35.

Eby, G.N., 1990. The A-type granitoids: A review of their occurrence and chemical characteristics and speculations on their petrogenesis. Lithos, 26(1-2), 115-134.

Eby, G.N., 1992. Chemical subdivision of the A-type granitoids: Petrogenetic and tectonic implications. Geology, 20(7), 641-644.

Ennih, N., Liégeois, J.P., 2008. The boundaries of the West African craton, with special reference to the basement of the Moroccan metacratonic Anti-Atlas belt. London, The Geological Society, 297(1, Special Publications), 1-17.

Eriksson, P.G., Mazumder, R., Catuneanu, O., Bumby, A.J., Ilondo, B.O., 2006. Precambrian continental freeboard and geological evolution: A time perspective. Earth-Science Reviews, 79(3-4), 165-204.

Frost, C.D., Frost, B.R., Chamberlain, K.R., Edwards, B.R., 1999. Petrogenesis of the 1.43 Ga Sherman batholith, SE Wyoming, USA: A reduced, rapakivi-type anorogenic granite. Journal of Petrology, 40(12), 1771-1802.

Frost, B.R., Barnes, C.G., Collins, W.J., Arculus, R.J., Ellis, D.J., Frost, C.D., 2001. A geochemical classification for granitic rocks. Journal of Petrology, 42(11), 2033-2048.

Frost, B.R., Frost, C.D., 2008. A geochemical classification for feldspathic igneous rocks. Journal of Petrology, 49(11), 1955-1969.

García-Arias, M., Camera, M.M., Dahlquist, J.A., Gao, P., Couzinié, S., Díez-Montes, A., 2024. The tectonic significance of peri-Gondwanan Late Neoproterozoic-Early Palaeozoic felsic peraluminous magmatism. Earth-Science Reviews,104803.

Goodge, J.W., Vervoort, J.D., 2006. Origin of Mesoproterozoic A-type granites in Laurentia: Hf isotope evidence. Earth and Planetary Science Letters, 243(3-4), 711-731.

Gorring, M.L., Estelle, T.C., Volkert, R.A., 2004. Geochemistry of the late Mesoproterozoic Mount Eve Granite suite: Implications for late to post-Ottawan tectonics in the New Jersey-Hudson Highlands. Geological Society of America Memoirs, 197, 505-523.

Han, B.F., Wang, S.G., Jahn, B.M., Hong, D.W., Kagami, H., Sun, Y.L., 1997. Depleted-mantle source for the Ulungur River A-type granites from North Xinjiang, China: Geochemistry and Nd-Sr isotopic evidence, and implications for Phanerozoic crustal growth. Chemical Geology, 138(3-4), 135-159.

Heilimo, E., Elburg, M.A., Andersen, T., 2014. Crustal growth and reworking during Lapland-Kola orogeny in northern Fennoscandia: U-Pb and Lu-Hf data from the Nattanen and Litsa-Aragub-type granites. Lithos, 205, 112-126.

Huang, X.L., Xu, Y.G., Li, X.H., Li, W.X., Lan, J.B., Zhang, H.H., Yang, Q.J., 2008. Petrogenesis and tectonic implications of Neoproterozoic, highly fractionated A-type granites from Mianning, South China. Precambrian Research, 165(3-4), 190-204.

Jung, S., Mezger, K., Hoernes, S., 1998. Petrology and geochemistry of syn-to post-collisional metaluminous A-type granites—a major and trace element and Nd-Sr-Pb-O-isotope study from the Proterozoic Damara Belt, Namibia. Lithos, 45(1-4), 147-175.

Jung, S., Hoernes, S., Mezger, K., 2000. Geochronology and petrogenesis of Pan-African, syn-tectonic, S-type and post-tectonic A-type granite (Namibia): Products of melting of crustal sources, fractional crystallization and wall rock entrainment. Lithos, 50(4), 259-287.

Kemp, A.I.S., Hawkesworth, C.J., Paterson, B.A., Kinny, P.D., 2007. Episodic growth of the Gondwana supercontinent from hafnium and oxygen isotopes in zircon. Nature, 439, 580-583.

Khanna, P.P., 2009. An appraisal of ICP-MS technique for determination of REEs: Long term QC assessment of silicate rock analysis. Him. Geol., 30, 95-99.

King, P., White, A., Chappell, B., Allen, C., 1997. Characterization and origin of aluminous A-type granites from the Lachlan Fold Belt, southeastern Australia. J Petrol, 38, 371-391.

King, P.L., Chappell, B.W., Allen, C.M., White, A.J.R., 2001. Are A-type granites the high-temperature felsic granites? Evidence from fractionated granites of the Wangrah Suite. Australian Journal of Earth Sciences, 48(4), 501-514.

Laurent, O., Martin, H., Moyen, J.F., Doucelance, R., 2014. The diversity and evolution of late-Archean granitoids: Evidence for the onset of "modern-style" plate tectonics between 3.0 and 2.5 Ga. Lithos, 205, 208-235.

Le Bas, M.J., Le Maitre, R.W., Streckeisen, A., Zanettin, B., 1986. A Chemical Classification of Volcanic Rocks Based on the Total Alkali-Silica Diagram. Journal of Petrology, 27(3), 745-750.

Loiselle, M., Wones, D., 1979. Characteristics and origin of anorogenic granites. Geological Society of America Abstracts with Programs, 468.

Lucas-Tooth, J., Pyne, C., 1964. The accurate determination of major constituents by X-ray fluorescent analysis in the presence of large interelement effects. Advances in X-ray Analysis, 7, 523-541.

Mahalik, N.K., 1994. Geology of the contact between the Eastern Ghats belt and North Orissa craton, India. Geological Society of India, 44(1), 41-51.

Mahalik, N.K., 1996. Lithology and tectonothermal history of the Precambrian rocks of Orissa along the eastern coast of India. Journal of Southeast Asian Earth Sciences, 14(3-4), 209-219.

Maniar, P.D., Piccoli, P.M., 1989. Tectonic discrimination of granitoids. Geological Society of America Bulletin, 101(5), 635-643.

Mazumder, S.K., 1978. Precambrian geology of eastern India between the Ganga and the Mahanadi-a review. Records of the Geological Survey of India, 110, 60-116.

Mazumder, R., 2005. Proterozoic sedimentation and volcanism in the Singhbhum crustal province, India and their implications. Sedimentary Geology, 176(1-2), 167-193.

Mazumder, R., Bose, P.K., Sarkar, S., 2000. A commentary on the tectono-sedimentary record of the pre-2.0 Ga continental growth of India vis-a-vis a possible pre-Gondwana Afro-Indian supercontinent. Journal of African Earth Sciences, 30(2), 201-217.

McCurry, M., Hayden, K.P., Morse, L.H., Mertzman, S., 2008. Genesis of post-hotspot, A-type rhyolite of the Eastern Snake River Plain volcanic field by extreme fractional crystallization of olivine tholeiite. Bulletin of Volcanology, 70, 361-383.

Miller, C.F., McDowell, S.M., Mapes, R.W., 2003. Hot and cold granites? Implications of zircon saturation temperatures and preservation of inheritance. Geology, 31(6), 529-532.

Mingram, B., Trumbull, R.B., Littman, S., Gerstenberger, H., 2000. A petrogenetic study of anorogenic felsic magmatism in the Cretaceous Paresis ring complex, Namibia: Evidence for mixing of crust and mantle-derived components. Lithos, 54(1-2), 1-22.

Moyen, J.F., 2009. High Sr/Y and La/Yb ratios: the meaning of the "adakitic signature". Lithos, 112(3-4), 556-574.

Moyen, J.F., Champion, D., Smithies, R.H., 2009. The geochemistry of Archaean plagioclase-rich granites as a marker of source enrichment and depth of melting. Earth and Environmental Science Transactions of the Royal Society of Edinburgh, 100(1-2), 35-50.

Mukhopadhyay, D., 2001. The Archaean nucleus of Singhbhum: The present state of knowledge. Gondwana Research, 4(3), 307-318.

Mukhopadhyay, J., Beukes, N.J., Armstrong, R.A., Zimmermann, U., Ghosh, G., Medda, R.A., 2008. Dating the oldest greenstone in India: A 3.51-Ga precise U-Pb SHRIMP zircon age for dacitic lava of the southern Iron Ore Group, Singhbhum craton. The Journal of Geology, 116(5), 449-461.

Mukhopadhyay, D., Matin, A., 2020. The architecture and evolution of the Singhbhum Craton. Episodes Journal of International Geoscience, 43(1), 19-50.

Namur, O., Charlier, B., Toplis, M.J., Higgins, M.D., Hounsell, V., Liégeois, J.P., Vander Auwera, J., 2011. Differentiation of tholeiitic basalt to A-type granite in the Sept Iles layered intrusion, Canada. Journal of Petrology, 52(3), 487-539.

Nash, C.R., Rankin, L.R., Leeming, P.M., Harris, L.B., 1996. Delineation of lithostructural domains in northern Orissa (India) from Landsat Thematic Mapper imagery. Tectonophysics, 260(4), 245-257.

Pandey, K.K., Pandey, U.K., Singh, Y., Malpe, D.B., 2018. Geochemistry and geochronology (Pb-Pb and Sm-Nd) of the Jharsuguda granitoids: implications for age of rare metal metallogeny in North Odisha. Exploration and Research for Atomic Minerals, 27, 171-181.

Pandit, M.K., Kumar, H., Wang, W., 2021. Geochemistry and geochronology of A-type basement granitoids in the northcentral Aravalli Craton: Implications on Paleoproterozoic geodynamics of NW Indian Block. Geosci Front, 12, 101084.

Pearce, J.A., Harris, N.B., Tindle, A.G., 1984. Trace element discrimination diagrams for the tectonic interpretation of granitic rocks. Journal of Petrology, 25(4), 956-983.

Pitcher, W.S., 1997. The nature and origin of granite. Springer Science & Business Media.

Rao, P., 1964. Stratigraphic relations of Precambrian iron formations and associated sedimentary sequences in parts of Keonjhar, Cuttack, Dhenkanal and Sundargarh districts of Orissa, India.

Rath, S.C., Behera, S.N., Som, S.K., 1993. Contact zone between Eastern Ghats and Iron ore Supergroup/Chhattisgarh Supergroup with special emphasis on Petrology and Mineral association in parts of Western Orissa in Sambalpur, Dhenkanal and Kalahandi district: Kansar-Jamankira area. Rec. Geol. Surv. India, 127(3), 50-52.

Saha, A.K., 1994. Crustal evolution of Singhbhum-north Orissa, eastern India. Mem. Geol. Soc. Ind., 27.

Saini, N.K., Mukherjee, P.K., Khanna, P.P., Purohit, K.K., 2007. A proposed amphibolite reference rock sample (AM-H) from Himachal Pradesh. Geological Society of India, 70(5), 799-802.

Saini, N.K., Khanna, P.P., Mukherjee, P.K., Purohit, K.K., 2014. Preparation and Characterisation of Two Geochemical Reference Materials: DG-H (Granite) and AM-H (Amphibolite) from the Himalayan Orogenic Belt. Geostandards and Geoanalytical Research, 38(1), 111-122.

Sarkar, S.N., Saha, A.K., 1962. A revision of the Precambrian stratigraphy and tectonics of Singhbhum and adjacent areas, Eastern India. Quarterly Journal of the Geological Mining and Metallurgical Society of India, 34, 97-133.

Sarkar, S.C., Gupta, A., 2012. Crustal evolution and metallogeny in India. Cambridge University Press.

Sethy, P.C., 2014. Structure, Stratigraphy and evolutionary history of Precambrian rocks of Jamankira -Kuchinda sector, Sambalpur district, Orissa. Ph.D. Thesis. Odisha, Sambalpur University, unpublished.

St-Onge, M.R., Van Gool, J.A., Garde, A.A., Scott, D.J., 2009. Correlation of Archaean and Palaeoproterozoic units between northeastern Canada and western Greenland: Constraining the pre-collisional upper plate accretionary history of the Trans-Hudson orogen. London, The Geological Society, 318(1, Special Publications), 193-235.

Sun, S.S., McDonough, W.F., 1989. Chemical and isotopic systematics of oceanic basalts: Implications for mantle composition and processes. London, The Geological Society, 42(1, Special Publications), 313-345.

Taylor, S.R., McLennan, S.M., 1981. The composition and evolution of the continental crust: Rare earth element evidence from sedimentary rocks. Philosophical Transactions of the Royal Society of London, Series A, Mathematical and Physical Sciences, 301(1461), 381-399.

Taylor, S.R., McLennan, S.M., 1995. The continental crust: Its composition and evolution. Black well Scientific publications.

Topno, A., Dey, S., Liu, Y., Zong, K., 2018. Early Neoarchaean A-type granitic magmatism by crustal reworking in Singhbhum craton: Evidence from Pala Lahara area, Orissa. Journal of Earth System Science, 127(3), 43.

Wang, L.X., Ma, C.Q., Zhang, C., Zhu, Y.X., Marks, M.A., 2018. Halogen geochemistry of I-and A-type granites from Jiuhuashan region (South China): Insights into the elevated fluorine in A-type granite. Chemical Geology, 478, 164-182.

Wang, Y., Yang, Y.Z., Siebel, W., Zhang, H., Zhang, Y.S., Chen, F., 2020. Geochemistry and tectonic significance of late Paleoproterozoic A-type granites along the southern margin of the North China Craton. Sci Rep, 10, 86.

Weaver, B.L., Tarney, J., 1984. Empirical approach to estimating the composition of the continental crust. Nature, 310(5978), 575-577.

Whalen, J., Currie, K., Chappell, B., 1987. A-type granites: Geochemical characteristics, discrimination and petrogenesis. Contrib Miner Petrol, 95, 407-419.

Whitney, D.L., Evans, B.W., 2010. Abbreviations for names of rock-forming minerals. American Mineralogist, 95, 185-187.

Windley, B.F., Whitehouse, M.J., Ba-Bttat, M.A., 1996. Early Precambrian gneiss terranes and Pan-African island arcs in Yemen: Crustal accretion of the eastern Arabian Shield. Geology, 24(2), 131-134.

Winter, J.D., 2014. Principles of igneous and metamorphic petrology. Pearson education, Harlow, UK.

Yang, J.H., Wu, F.Y., Chung, S.L., Wilde, S.A., Chu, M.F., 2006. A hybrid origin for the Qianshan A-type granite, northeast China: Geochemical and Sr-Nd-Hf isotopic evidence. Lithos, 89(1-2), 89-106.

Zhang, C.L., Zou, H.B., 2013. Permian A-type granites in Tarim and western part of Central Asian Orogenic Belt (CAOB): Genetically related to a common Permian mantle plume? Lithos, 172, 47-60.

Zhong, H., Zhu, W.G., Chu, Z.Y., He, D.F., Song, X.Y., 2007. Shrimp U-Pb zircon geochronology, geochemistry, and Nd-Sr isotopic study of contrasting granites in the Emeishan large igneous province, SW China. Chemical Geology, 236(1-2), 112-133.

Zhu, W.G., Zhong, H., Li, X.H., He, D.F., Song, X.Y., Ren, T., Liao, J.Q., 2010. The early Jurassic mafic-ultramafic intrusion and A-type granite from northeastern Guangdong, SE China: Age, origin, and tectonic significance. Lithos, 119(3-4), 313-329.

Manuscript received January 2025;
revision accepted June 2025;
published Online October 2025.